Arab J. Nucl. Sci. Appl., Vol. 56, 5, 96-104 (2023)

ISSN 1110-0451

Arab Journal of Nuclear Sciences and Applications

Web site: ajnsa.journals.ekb.eg

(E S N S A)

Effect of Gamma Dose on Dielectric and Optical Properties of ZnO/PVA

Fatma Abdel Maged [(1,2)]

[(1)] *Canal High Institute of Engineering and Technology Suez, Egypt*
[(2)] *Elmenofia Higher Institute of Engineering and Technology, Elmenofia, Egypt*

ARTICLE INFO

Article history:

Received: 3rd Feb. 2023
Accepted: 19th Feb. 2021
Available online: 8th June 2023

Keywords:

Zinc Oxide (ZnO);
Wemple and Di-Domenico;
Optical Properties;
Electrical Properties.

ABSTRACT

Zinc oxide ZnO was synthesized via a sol-gel process, incorporated with polyvinyl alcohol (PVA) using the casting method. Different doses of gamma radiation (20,30,40 and 50) irradiated the ZnO /PVA composite. The structured shape of ZnO was examined by (HRTEM). The optical direct transition band gap was reduced from (3.25 to 2.7 eV) for (20 kGy to 40 kGy) due to limited states' influence in the forbidden band. The refractive index was examined using Wemple and Di-Domenico method. The dispersion energy E_d and the oscillator energy E_o are related to variations in the structural order of the ZnO/PVA by irradiation dose. The dielectric loss tangent ($tan\delta$), dielectric constant (ε'), and AC electrical conductivities of ZnO PVA samples have been recorded. Finally, it was noticed that the A.C. electrical conductivity appears to change exponentially with frequency, and this behavior is due to significant charge carrier migration via the hopping mechanism. The nanocomposite has a specific capacitance value of 36.7 F/g and 91.75 F/g, which makes it a good candidate for optoelectronic applications.

1. INTRODUCTION

The use of polymer composite systems has been steadily increasing, due to their numerous potentials uses in the fields of sensors, dielectrics, bioplastics, biomedical applications, and coatings [1-2]. ZnO QDs are of major significance due to their notable characteristics, such as a wide direct energy gap of around 3.4 eV at ambient temperature, a significant exciton binding energy of 60 meV, and nontoxicity [3] A variety of synthetic methods for the preparation of ZnO, such as sol-gel process, direct precipitation, plasma synthesis, hydrothermal technique, synthesis via microwave and vapor transport process [4]. Polyvinyl alcohol (PVA) has magnificent physical properties, such as a semi-crystalline structure, water-solubility, low toxicity, low cost, and limited electrical conductivity [5]. ZnO nanostructures can be added to the polymer matrix to change the films' conductive, mechanical, electrical, and optical properties. Inorganic nanoparticles that are distributed in polymers have recently been the subject of extensive research [6]. The useful qualities of these inorganic-organic materials include strength, chemical and thermal permanence, elasticity, and dielectric properties. The most important aspect influencing the final product's qualities during the creation of nanocomposites is the interface coulomb interactions between the nanoparticle and the polymer functional groups [7]. (**Hameed et al.,)** [8] have reported the synthesis of the polymer nanocomposite (CMC/PEO-ZC NC) films. With the addition of ZC NC up to 2 wt%, the dielectric properties and conductivity of the polymer nanocomposite films were enhanced. (**Kanavi et al.,) [9]** have demonstrated that composite films made of polyvinyl alcohol and polyaniline varied in the proportion of zinc oxide (ZnO). The impedance analyzer's electrical conductivity graphs within frequency demonstrate that the samples' increased concentration and temperature led to enhanced conductivity in the films. (**Mohammed et al.,) [**10] have studied those membranes made of ZnO/PMMA nanocomposite (PNC) with varying zinc oxide nanoparticle contents. Enhanced ZnO nanoparticle loading (ZnO NP) results in higher values of the dielectric constant due to increased polarization in the polymer matrix at a lower frequency.

This paper aims to synthesize (ZnO) nanoparticles via the sol-gel technique. The authors prepared ZnO/PVA nanocomposite films by the casting method. ZnO)/PVA

Corresponding author: fatmamaged@science.zu.edu.eg
DOI: 10.21608/ajnsa.2023.191570.1716

nanocomposite films were irradiated at Gamma doses (20,30,40 and 50kGy). ZnO was examined using HRTEM analysis. UV-vis spectroscopy, bandgap, and dispersion of refractive index of (ZnO)/PVA nanocomposites were investigated by Tauck's, Wemple–DiDomenico (W–D) model. The dielectric and electrical conductivity properties were studied for (ZnO)/PVA nanocomposite films. The cyclic voltammetry was investigated for ZnO/PVA films.

2. EXPERIMENTAL

2.1 Materials

PVA was purchased from TECHNO PHARMCHEM, INDIA. zinc nitrate hexahydrate (Zn $(NO_3)_2$6H2O and citric acid, were obtained from (PIOCHEM) All chemicals were utilized with extra purity.

2.2. Synthesis of (ZnO) nanoparticle

ZnO nanoparticles were synthesized utilizing the sol-gel technique. Under steady stirring, the zinc nitrate hexahydrate (Zn $(NO_3)_2$6H_2O) was dissolved in distilled water and heated to roughly 90ºC for one hour. The citric acid was added to the mixture while keeping the citric acid to zinc nitrate hexahydrate molar ratio at 1:1. To establish good homogeneity, this combined solution was then agitated for two hours. The precursor mixture was heated to facilitate evaporation at 100 ºC for 24 hours, followed by combustion at 550 ºC for 2 hours, to produce zinc oxide (ZnO).

2.3. synthesis of ZnO / PVA films

First, 40 ml of deionized water was used to dissolve 4g of polyvinyl alcohol (PVA) powder over the time of three hours at 70°C while stirring. Second, under steady magnetic stirring, a 0.2g of ZnO powder was added to the PVA solution[1]. The nanocomposite film was then produced by casting each blend into a Petri dish. The ZnO / PVA nanocomposite films were irradiated with gamma doses (20,30,40 and 50 kGy).

3. CHARACTERIZATION

To display composite particle size distribution and geometry, a high-resolution transmission electron microscope (HRTEM) model (JEOL/JME-2100, Japan) was employed. The optical characteristics of films were investigated using a spectrophotometer (Spectro UV-VIS 2800, USA). The findings of the cyclic voltammetry (CV) study were assessed (kitheily 4200-SCS). The current at the employed electrode is placed against the utilized voltage (the working electrode's potential) to obtain the cyclic voltammogram trace. Cyclic voltammetry is used to investigate the electrochemical characteristics of a solution or a molecule adsorbed onto an electrode. Using a Novo control alpha-A analyzer at room temperature, films were examined electrically in the frequency band of 10^{-1} - 10^{7} Hz. The samples for the dielectric study were located between the two gold-plated electrodes in a parallel plate geometrical configuration (20 mm). The used voltage was kept constant at 0.2 V.

4-RESULTS AND DISCUSSION

4.1 HR-TEM analysis

Fig 1 illustrates the (HR-TEM) image of the ZnO nanoparticle. It can be noticed that ZnO has a spherical shape with an average particle size of 25 nm. This confirmed the formation of ZnO nanoparticles.

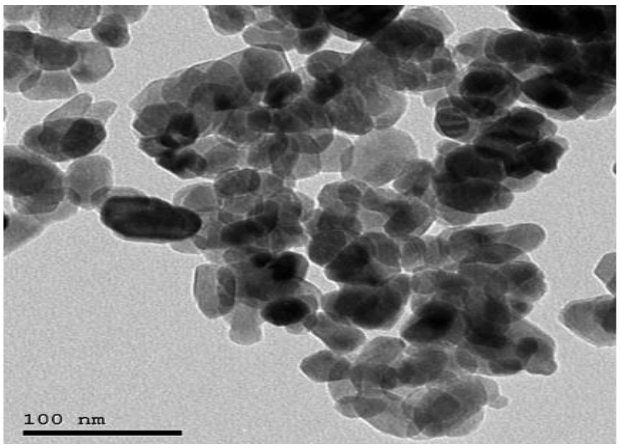

Fig. (1): The HR-TEM image of ZnO nanoparticles.

4.2 Dielectric and electrical properties

This method (Broadband Dielectric Spectroscopy, BDS) is employed to evaluate the complex conductivity function, σ*(υ), as well as the complex dielectric function, ε* (υ). The relationship between these variables can be seen in the equation below. [11]

$$\varepsilon^*(\omega) = \varepsilon'(\omega) - i\varepsilon''(\omega) \quad \textbf{(1)}$$

$$\sigma^*(\omega) = i\varepsilon_0\,\omega\varepsilon^*(\omega) \quad \textbf{(2)}$$

Suggesting that: $\boldsymbol{\sigma' = \varepsilon_o \omega \varepsilon''},\ \boldsymbol{\sigma'' = \varepsilon_o \omega \varepsilon'}$

($\omega = 2\pi\upsilon$) is the circular frequency and ε_o is the vacuum permittivity).

This type of spectroscopy is a unique identifier of the sample under investigation, just like any other type of spectroscopy. It varies from them, though, in that it has a wide variety of frequencies. This causes the dielectric spectrum to be split into three categories microscopic molecular dynamics, charge carrier mobility, which is demonstrated by conductivity mechanisms, and

accumulation of charge carriers at interfaces, such as those between the phases of multi-component composites and at the interface between electrodes and dielectric materials. Figure 2 shows a graphic representation of the estimated permittivity of the synthesized films versus frequency. The permittivity's resonance ε′, reveals a striking influence on the frequency window during an investigation. Since all curves are crushed together, the image was unable to depict the extraordinary impact of irradiation dose on permittivity. Two prominent dynamics of the real part of complex permittivity, ε′, might be seen here as represented against frequency. The frequency range (0.1Hz – 10 kHz) displays a steady reduction of 6 powers of magnitudes, owing to charge carrier transport, which results in high conductivity. This behavior screened out any dispersion step and hence dynamic relaxation peak on the dielectric loss spectra, ε″ (ν), which shows a simple linear decrease with increasing frequency, at larger frequency ranges (that is from 10 kHz up to 20 MHz) a very small result of frequency on diminishing the permittivity. This reflects that the influence of all forms of polarization changes lags behind the frequency of the used external electric field at higher frequencies. The inset shows the numerical values taken at two spot frequencies, namely 1 Hz and 1 MHz. The permittivity values at the two selected frequencies taken as a representative example are very close at all the doses of irradiation under consideration. The relatively higher value was found at 40kGy irradiated sample and the lower at 30kGy. This confirms that the composite response is mainly due to the irradiation process but not to the dose of irradiation, at least in the considered range of irradiation.

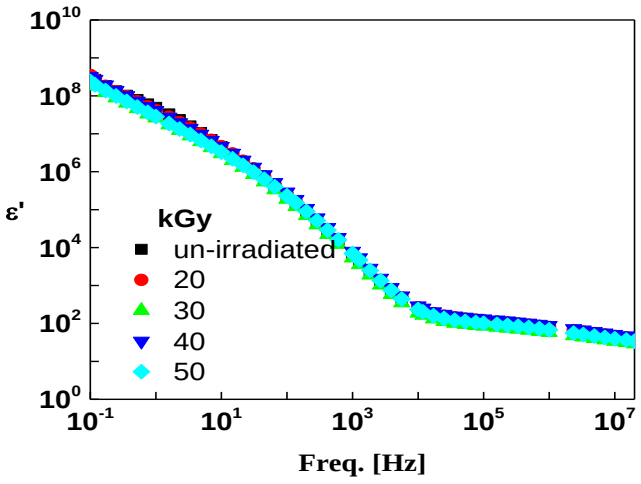

Fig. (2): The frequency dependence of the permittivity, ε′ for the five investigated samples as indicated.

The dissipation factor tan δ and the ac-conductivity are illustrated graphically in figure 3 against frequency (log-log scale) for the investigated irradiated nanocomposites. The figure shows a distinct, sharp peak at the lower limit points of frequency, which is accompanied by a slight shoulder., and the maximum peak position is at about 10 kHz. On the other hand, the ac-conductivity, σ′, versus frequency, shows three different trends similar to that found recently in many other conductive polymer composites and dielectric materials [12-17]. It satisfies the power law at higher frequencies: $[\sigma'(\omega) = A\omega^s]$, where A is constant and s is the rate of fluctuation of AC conductivity with growing frequency. The dc-conductivity, σ_{dc} is determined by a plateau-like behavior in the mid-frequency region. The change in the irradiation dose causes it to fluctuate slightly between 1 and 2 mS/cm. The conductivity effect has a significant role in the permittivity values. The peak position of tan δ is accompanied by a minimum on the frequency reliance on the imaginary part of complex conductivity (usually called onset frequency ν_{on}, Fig. 4 shows the starting point of building up the electrochemical double layer at the composite/metal electrode interphase. The maximum peak position of σ″, as presented against frequency in figure 4, shows that the electrochemical double layer (ECDL) construction is completed.

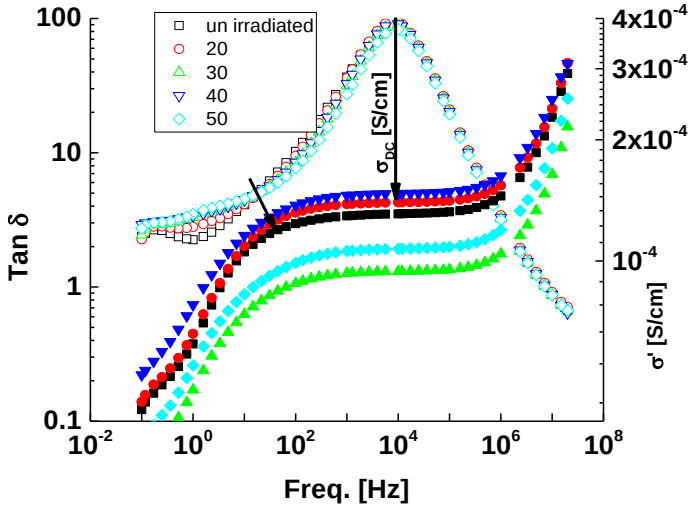

Fig. (3): The variation of dissipation factor (tan δ) open and AC-conductivity (σ_{ac}) close symbols, as presented versus frequency for the irradiated nanocomposites. The same notations as in figure 2.

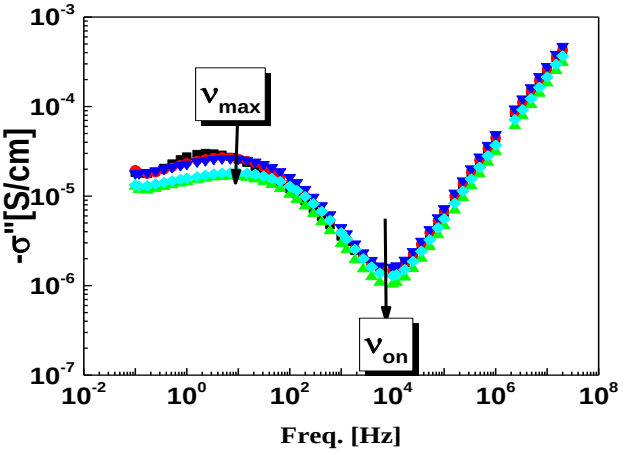

Fig. (4): The variation of the imaginary part of complex conductivity, σ″ , as presented versus frequency for the irradiated nanocomposites. The same notations as in figure 2.

Because the accumulation of charge carriers at the interface is the source of electrode polarization, it requires quantitative evaluation. This widespread phenomenon happens at the interface between a metallic and an ionic conductor when the sample cell's overall dielectric response multiplies by several orders of magnitude. Ion mobility at the interfaces is severely constrained by Coulombic interactions; this assumption statistically identifies the discovered scaling laws. It enables the assumption of the bulk conductivity of the investigated ionic charge carriers via a novel formula. These samples could be the subject of additional research, such as a study of how temperature affects electrical and dielectric properties, which may reveal details on the fluctuation dynamics of the charge carriers accumulated at the interface. The asymmetric wing of the σ″ peak at low values of frequencies, joined by a shoulder in the tanδ and deviation from linearity of conductivity reduction, as gotten in figure 3, occurs as a consequence of these fluctuation dynamics. This study shows that these samples are promising in the technology of electrical storage energy. The electric modulus procedure, M*, was utilized to analyze the conductivity data in conductive polymer composites and ionic polymeric materials like PVA and reduce the electrode influence. The equation defines the complex electric modulus, M* in ref [1-2].

Fig. 5. (a,b) displays the dispersion of M' *and* M'' against log *f* for irradiated samples.

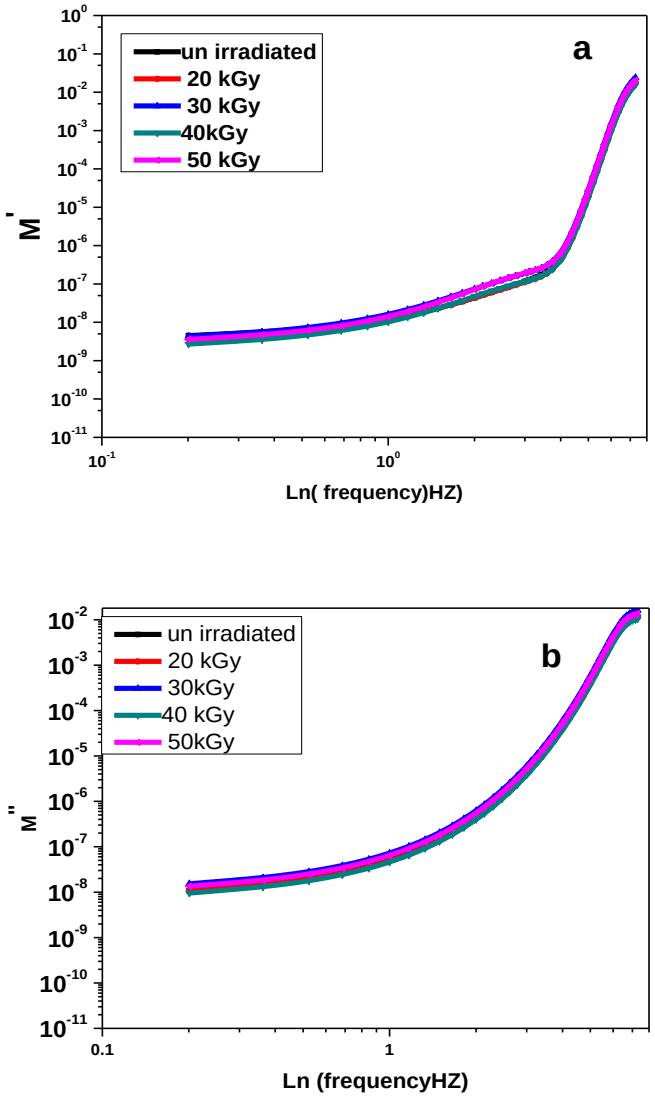

Fig. (5): Dispersion of M' *and* M'' as a function of log *f* for irradiated samples.

4.3 Optical properties

Fig. 6 shows the measured absorbance, A, values for the irradiated samples as a function of wavelength. It is seen that the absorption band of PVA at 280 nm and a new absorption band emerged in the region 320 nm due to the combining of ZnO in PVA [18]. This could be ascribed to the inserted ZnO NPs' surface Plasmon resonance (SPR) absorption band, which is related to the collective oscillations' resonance for the electrons in the conduction band of Zn NPs when paired with incident electromagnetic radiations[19][20]. The absorption of PVA/Zn samples increases with increasing gamma dose irradiation (20 and 50 kGy); the maximum gamma dose is 40kGy.

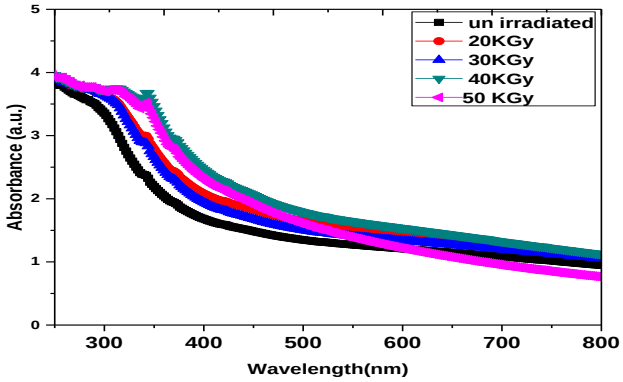

Fig. (6): The absorbance, A, values for the irradiated samples as a function of wavelength.

Fig.7 depicts the optical transmittance spectra for irradiated samples versus wavelength for various gamma doses. It is noticed that the transmittance of the samples decreases with increased doses except the 50 kGy dose. The optical absorption coefficient (α) provides a better understanding of the electronic band structure of a solid material. It is one of the essential characteristics affected by the incident wavelength. Fig. 8 displays the optical absorption coefficients of the irradiated samples as a function of (hυ) eV at various gamma doses, which can be calculated using Beer–formula Lambert's [21]

$$\alpha = \frac{2.303A}{t} \qquad (3)$$

Where A is the absorbance and t is the film thickness. It is proven that as the gamma dose rises, the value of absorption grows, representing more light absorption in the larger dosage. This graph shows an irregularity near the E_{edge} that then increase quickly in a line relationship (the maximum value at 30 kGy and 50 kGy does). This rapid increase in α is due to the inter-band transitions with photons energy[22]. The absorption process is dependent on a photon with enough energy to allow electrons to transfer from valence bands with low energy to conduction bands with high energy. The energy gap (E_g), which plays an essential role in optoelectronic design and new solar cells, is one of the most critical variables in determining the unique characteristics of solid materials. As a result, a precise assessment of its evaluation value is required, which can be accomplished by analyzing the absorption spectra of the optical samples under consideration. The abs are used to calculate E_g by Mott and Davis formula, which is used to convert the absorption spectrum into Tauc's plot [23]

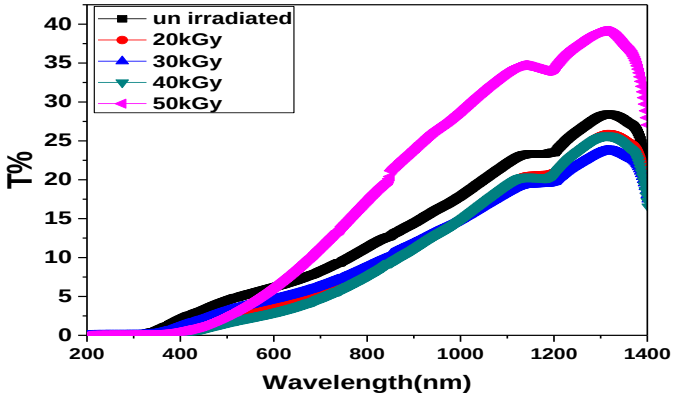

Fig. (7): The optical transmittance spectra for irradiated samples versus wavelength for various gamma doses.

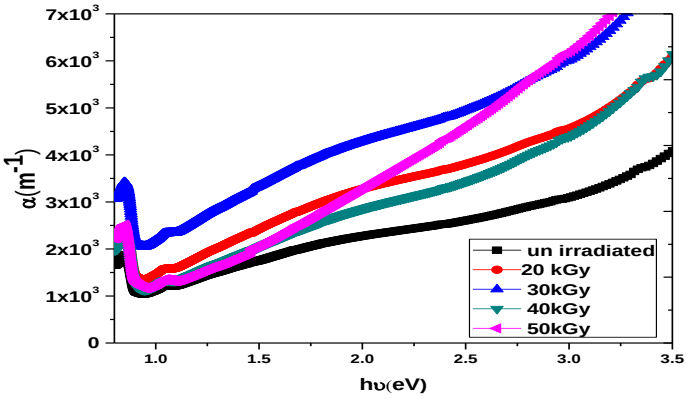

Fig. (8): The optical absorption coefficients of the irradiated samples as a function of (hυ) eV at various gamma doses.

Fig. 9. illustrates the correlation between $(\alpha h\upsilon)^2$ versus (hυ) for irradiated samples by varied gamma dose. E_g, values for irradiated samples are tabulated in Table 1 for various gamma doses. With increasing the gamma dose, it is seen that the value of E_g reduces from (3.25 to 2.7 eV)for (unirradiated to 50 kGy)it is matched with other literature [19][24].

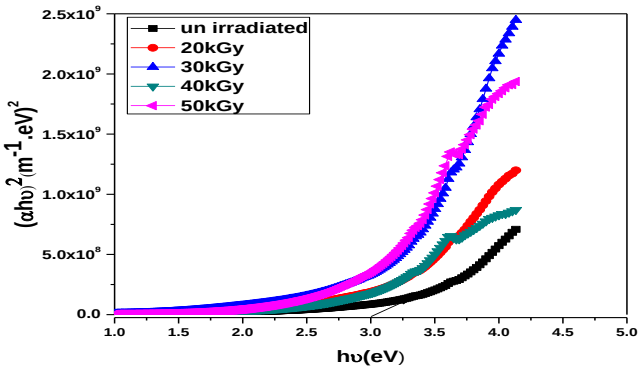

Fig. (9): The variation of (αhυ)2 versus (hυ) for irradiated samples by varied gamma dose.

Table (1): Energy band gap, Optical dispersion, and nonlinear parameters of irradiated samples.

Samples	E_g eV	E_d eV	E_o eV	n_o	$X^{(1)}$	$X^{(3)}$	$n^{(2)}$
Un irradiated	3.25	7.5	8.71	1.976	0.068	3.766*10^-15	9.272*10^-12
20 kGy	3	3.53	8.24	2.1	0.034	2.297*10^-16	1.66*10^-11
30 kGy	3	-	-	-	-	-	-
40 kGy	2.7	7.5	7.5	3.32	0.068	3.74*10^-15	7.8*10^-10
50 kGy	2.7	7.62	7.62	8.39	0.0583	1.96*10^-15	7.099*10^-7

Attempting to understand the effects of gamma irradiation explains this observation. The radiolytic electrons or holes produced by this irradiation become trapped in the host matrix and form defect centers. As a result, new localized energy states arise between the energy bands in the host material matrix, resulting in a low energy gap or more absorption[24].

The refractive (n) and extinction (k) coefficients are essential attributes for analyzing optoelectronic components. The following equations can be used to achieve both of them[23].

$$n = \frac{1+\sqrt{R}}{1-\sqrt{R}} \quad (4)$$

$$k = \frac{\alpha\lambda}{4\pi} \quad (5)$$

Fig.10 Outlines The dependence of the extinction coefficient on incident light wavelengths for the irradiated samples. The extinction coefficient increases in the wavelength range 300-350 nm (U.V. region) and is constant in the wavelength range 400–800 nm (visible region) as the gamma dose increase. Fig.11 Shows the variation of (n) versus wavelength(nm) for irradiated samples. It is seen that the values of n increase with increased gamma dose from (1.15 to 1.35) for (20 kGy to 50 kGy). This increase is linked to a change in polymeric structure. Furthermore, gamma irradiation of samples increases the number of inter-chain contacts, resulting in changes in packing density, molecular weight distribution, and refractive index as the irradiation dose increases [25].

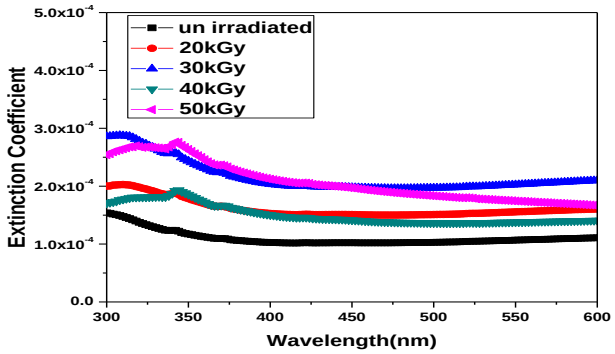

Fig. (10): The dependence of the extinction coefficient on incident light wavelengths for the irradiated samples

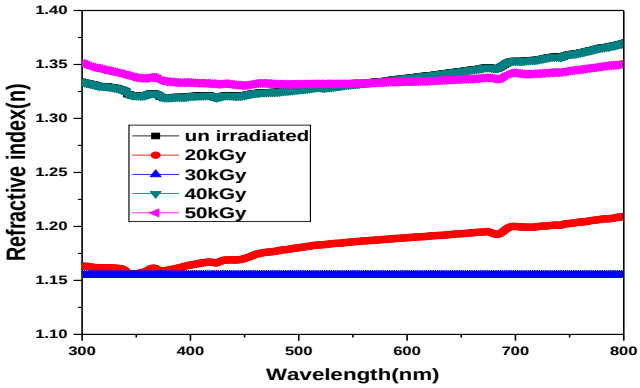

Fig. (11): the variation of (n) versus wavelength(nm) for irradiated samples.

The oscillator energy E_0 and dispersion energy E_d for irradiated samples may be estimated and stated using the single oscillator model(the Wemple and DiDomenico model)[26]

$$\frac{1}{n^2-1} = \frac{E_0}{E_d} - \left(\frac{1}{E_0 E_d}\right)(h\upsilon)^2 \quad (6)$$

$$n_0 = \left(1 + \frac{E_d}{E_0}\right)^{1/2} \quad (7)$$

Fig. 12. represents the variation between ($1/n^2$-1) and the photon energy square for irradiated samples. The estimated E_0, E_d, and n_0 for the samples are recorded in Table 1. The influence of gamma-irradiation on the oscillator energy and dispersion energy may be understood.

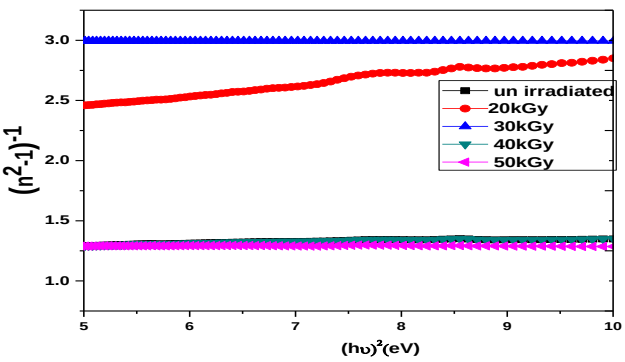

Fig. (12): The variation between (1/n2-1) and the photon energy square for irradiated samples.

Also, the nonlinear parameters can be calculated using the values of E_d, E_0, and n_0 from the following equations[26].

$$x^{(1)} = \frac{E_d}{4\pi E_0} \quad \textbf{(8)}$$

$$x^{(3)} = 6.82 * 10^{-15}(\frac{E_d}{E_0})^4 \quad \textbf{(9)}$$

$$n^{(2)} = 12\pi \frac{x^{(3)}}{n_0} \quad \textbf{(10)}$$

The optical response of a material is mostly examined related to optical conductivity (σ), which is the electrical conductivity that comes from the movement of charge carriers caused by the incident electromagnetic waves' oscillating electric field. The following equation can be used to express the optical conductivity[23].

$$\sigma_{opt} = n\alpha c/4\pi \quad \textbf{(11)}$$

Fig. 13 illustrates the optical conductivity of irradiated samples concerning incident photon energy. It is seen that the optical conductivity grows as the energy of the incident photon increases. At low frequencies, optical conductivity tends to have steady values. This is due to the sample receiving inadequate energy to excite the electrons. The optical conductivity improves as hυ increases.[27-28]. This is due to the incident energy being appropriate to excite electrons from one state to another, increasing the number of free charge carriers. Furthermore, the decreasing crystalline degree of the polymer films causes an increase in polymer matrix disordering and the creation of a localized tail state in the band gap.

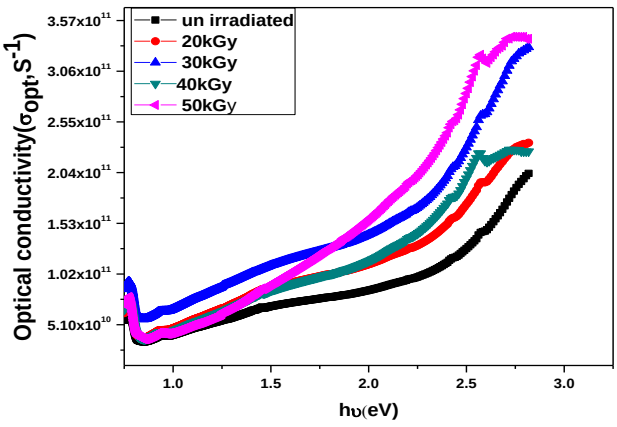

Fig. (13): The optical conductivity of irradiated samples as a function of incident photon energy.

4.4 Electrochemical analysis

One essential characteristic that determines a material's potential is electrochemical analysis to investigate the ZnO/ PVA composite electrode's electrochemical reactions. Fig.14 displays the variation in CV behavior for ZnO/ PVA at 40kGy recorded from 1.1 to −0.10 V at a scanning rate of 20 mV s^{-1} and 50 mV s^{-1}. The anodic peak at 0.7 V can be seen on the cyclic voltammetry of the ZnO/ PVA composite electrode. The specific capacitance from a CV in F/g was determined using an equation [29]

$$C_s = \frac{A}{2mk(V_2 - V_1)} \quad \textbf{(12)}$$

where A is the CV area, m is the active material's mass in grams (g), k is the scan rate in millivolts per second (mV/s), and V is the potential window (V). The ZnO/ZnS/PVA nanocomposite has a Cs value of 36.7 F/g and 91.75F/g at 50 mV s^{-1} and 20 mV s^{-1}. Using this composite can enhance the features of supercapacitors.

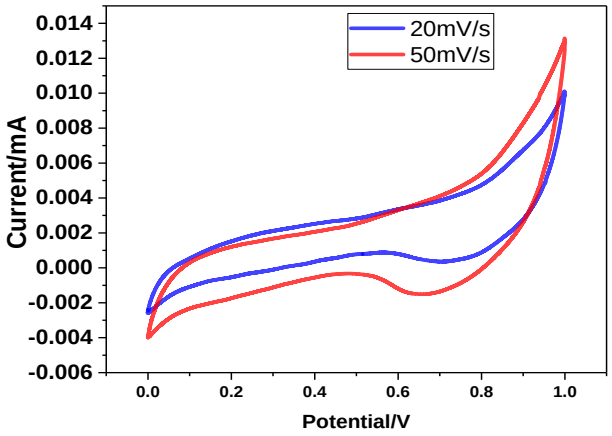

Fig. (14): The variation in CV behavior for nanocomposite at 40 kGy.

5. CONCLUSION

The synthesis of ZnO was presented by the sol-gel method. ZnO/ PVA nanocomposites synthesize by casting method and irradiated by gamma ray with different doses. HRTEM revealed the formation of ZnO nanoparticles with a mean size of 30 nm The optical absorption of the ZnO/PVA matrix was enhanced due to the formation of sub-levels in the forbidden band via increasing dose. Due to the interaction between PVA and ZnO, the dielectric constant and electrical conductivity properties were improved. Finally, from ac conductivity data analysis, it was noticed that electrical conductivity appears to change exponentially with frequency. This behavior is due to significant charge carrier migration via the hopping mechanism. The nanocomposite has a Cs value of 36.7 F/g and 91.75 F/g. The present

polymeric films are useful for a wider range of optoelectronics and electrical applications.

REFERENCES

[1] Maged, F.A., Shawkey, H.A., Rayan, D.A. and Turky, G.M. (2022) Comparative study of CdS & TiO_2 based polyaniline/polyvinyl alcohol nanocomposites as electrode for supercapacitors. *Physica Scripta*, **97** (11), 115805. DOI 10.1088/1402-4896/ac95e0

[2] Ashery, A. and Maged, F.A. (2022) Novel Structure, Electric and Dielectric Properties of PPy-PANI-GO-MWCNTs Composite/MnO2/Fe3O4/n-Si Structure. *ECS Journal of Solid State Science and Technology*, **11** (11), 115004. DOI 10.1149/2162-8777/ac9f67

[3] Ahmad, N., Majid, W.A., Zaini, M.S., Rosli, A.K., Adnan, R.H. and Halim, N.A. (2023) Energy harvesting performance of a novel polymer-nanocrystal composite of P (VDF-TrFE)/ZnO QD films. *Materials Science and Engineering*, B, 289, 116256. https://doi.org/10.1016/j.mseb.2022.116256

[4] Kanavi, P.S., Meti, S., Fattepur, R.H. and Patil, V.B. (2022): Emphasized temperature dependent electrical properties study of fabricated ZnO/PVA/PANI nanocomposite films. *Open Nano*, 7, 100057. https://doi.org/10.1016/j.onano.2022.100057

[5] Ali, H.E., Abdel-Aziz, M.M., Khairy, Y., Zahran, H.Y., Algarni, H., Yahia, I.S. and Sanaa, M.F. (2021) Microstructure analysis and nonlinear/linear optical parameters of polymeric composite films based PVAL for wide optical applications. *Physica Scripta*, **96**(11), 115804. DOI 10.1088/1402-4896/ac13e3

[6] Sahoo, R., Mishra, S., Ramadoss, A., Mohanty, S., Mahapatra, S. and Nayak, S.K. (2020) Temperature-dependent dielectric properties of metal-doped ZnO nanofiller reinforced PVDF nanocomposites. *Materials Research Bulletin*, **132**, 111005. https://doi.org/10.1016/j.materresbull.2020.111005

[7] Mohammed, M.I. (2022) Dielectric dispersion and relaxations in (PMMA/PVDF)/ZnO nanocomposites. *Polymer Bulletin*, **79** (4), 2443-2459. https://doi.org/10.1007/s00289-021-03606-z

[8] Hameed, S.T., Qahtan, T.F., Abdelghany, A.M. and Oraby, A.H. (2023) ZnO/CuO nanocomposite-based carboxymethyl cellulose/polyethylene oxide polymer electrolytes for energy storage applications. *Journal of Materials Research and Technology*,. **22**, 531-540. https://doi.org/10.1016/j.jmrt.2022.11.118

[9] Wang, Z., Bockstaller, M.R. and Matyjaszewski, K. (2021): Synthesis and applications of ZnO/polymer nanohybrids. *ACS Materials Letters*, **3** (5), 599-621. https://doi.org/10.1021/acsmaterialslett.1c00145

[10] Mohammed, M.I., Khafagy, R.M., Hussien, M.S., Sakr, G.B., Ibrahim, M.A., Yahia, I.S. & Zahran, H.Y. (2022) Enhancing the structural, optical, electrical, properties and photocatalytic applications of ZnO/PMMA nanocomposite membranes: Towards multifunctional membranes. *Journal of Materials Science: Materials in Electronics*, **33** (4), 1977-2002. https://doi.org/10.1007/s10854-021-07402-3

[11] Youssef, A.M., Abd El-Aziz, M.E., Abd El-Sayed, E.S., Moussa, M.A., Turky, G. & Kamel,S. (2019) Rational design and electrical study of conducting bionanocomposites hydrogel based on chitosan and silver nanoparticles. *International Journal of Biological Macromolecules*, 140, 886-894.

[12] Turky, G., Moussa, M.A., Hasanin, M., El-Sayed, N.S. and Kamel, S. (2021) Carboxymethyl cellulose-based hydrogel: dielectric study, antimicrobial activity and biocompatibility. Arabian *Journal for Science and Engineering*, **46** (1), 17-30.

[13] Sangoro, J., Cosby, T. and Kremer, F. (2016) "Rotational and translational diffusion in ionic liquids." *Dielectric Properties of Ionic Liquids*. Springer, Cham, 2016. 29-51.

[14] El-Sayed, N.S., Moussa, M.A., Kamel, S. and Turky, G. (2019) Development of electrical conducting nanocomposite based on carboxymethyl cellulose hydrogel/silver nanoparticles@ polypyrrole. *Synthetic Metals*, **250**, 104-114.

[15] Sangoro, J.R. and Kremer, F. (2012) Charge transport and glassy dynamics in ionic liquids. *Accounts of Chemical Research*, **45(** 4), 525-532.

[16] Omara, S.S., Turky, G., Ghoneim, A., Thünemann, A.F., Rehim, M.H.A. and Schönhals, A. (2017) Hyperbranched poly (amidoamine)/kaolinite nanocomposites: structure and charge carrier dynamics. *Polymer*, **121**, 64-74.

[17] Dacrory, S., Abou-Yousef, H., Kamel, S. and Turky, G. (2019) Development of biodegradable semiconducting foam based on micro-fibrillated cellulose/Cu-NPs. *International Journal of Biological Macromolecules*, **132**, 351-359.

[18] Mansour, A.F., Abdo, M.A., Maged, F.A. and Agag, G.M. (2021) Synthesis, Optical Properties and

Stabilization of ZnS Quantum Dots by Polymeric Matrices. *J. Inorg. Organomet. Polym. Mater.*, **31** (4), 1443–1450, 2021, DOI: 10.1007/s10904-021-01884-8.

[19] Alshahrani, B., ElSaeedy, H.I., Fares, S., Korna, A.H., Yakout, H.A., Maksoud, M.I.A. and Awed, A.S. (2021) The effect of gamma irradiation on structural, optical, and dispersion properties of PVA/Zn0. 5Co0. 4Ag0. 2Fe2O4 nanocomposite films. *Journal of Materials Science: Materials in Electronics*, **32**(10), 13336-13349., DOI: 10.1007/s10854-021-05913-7.

[20] Wiguna, P.A., Djuhana, D., Imawan, C. and Umar, A. (2020) Physicochemical properties of colloidal Ag/PVA nanoparticles synthesized by gamma irradiation. *J. Phys. Conf. Ser.*, **1428** (1), DOI: 10.1088/1742-6596/1428/1/012022.

[21] Menazea, A.A. (2020) One-Pot Pulsed Laser Ablation route assisted copper oxide nanoparticles doped in PEO/PVP blend for the electrical conductivity enhancement. *J. Mater. Res. Technol.*, **9** (2), 2412–2422, 2020, DOI: 10.1016/j.jmrt.2019.12.073.

[22] Ali, H.E. and Khairy, Y. (2020) Facile synthesis, structure, AFM, thermal, and optical analysis of BiI3/PVAL nanocomposite films for laser CUT-OFF optical devices. *Vacuum*, **180**, no. May, p. 109640, DOI: 0.1016/j.vacuum.2020.109640.

[23] Mansour, A.F., Elfalaky, A. and Maged, F.A. (2015) Synthesis, Characterization and Optical properties of PANI/ PVA Blends. *IOSR J. Appl. Phys.*, **7** (4), 37–45, 2015, DOI: 10.9790/4861-07433745.

[24] Salah, M., Gad, M., Elkattan, M. and Sabry, Y.M. (2020) Effect of gamma-irradiation and doping on the absorption edge and the optical bandgap of silver-doped PVA films.*Opt. Commun.*, **473**, October 2019, p. 125933, DOI: 10.1016/j.optcom.2020.125933.

[25] Chahal, R.P., Mahendia, S., Tomar, A.K. and Kumar, S. (2012) γ-Irradiated PVA/Ag nanocomposite films: Materials for optical applications. *J. Alloys Compd.*, vol. 538, pp. 212–219, 2012, DOI: 10.1016/j.jallcom.2012.05.085.

[26] Ali, H.E., Khairy, Y., Sayed, M.A., Algarni, H., Shkir, M., & Maged, F.A. (2022) Tailoring the linear/nonlinear optical and visible shielding performance of PVP/PVOH incorporated with NiO nanoparticles for optical devices. *Optik*, **251**, 168373.

[27] Soliman, T.S., Zaki, M.F., Hessian, M.M. and Elkalashy, S.I. (2021) The structure and optical properties of PVA-BaTiO3 nanocomposite films. *Opt. Mater. (Amst).*, **111**, no. October, p. 110648, DOI: 10.1016/j.optmat.2020.110648.

[28] Maged, F.A. and Mansour, A.F. (2022) The enhancement of the optical properties of CdS/PMMA by adding fullerence C60. *Physica Scripta Phys. Scr.*, 97 075802 https://doi.org/10.1088/1402-4896/ac7175.

[29] Elsonbaty, A., Harb, M., Soliman, M., Ebrahim, S. and Eltahan, A. (2021) Metal organic framework/layer double hydroxide/graphene oxide nanocomposite supercapacitor electrode. *Applied Physics Letters*, **118** (2), 023901.